Supporting Online Material

Oscillatory Thermo-Mechanical Instability of an Ultrathin Catalyst

By Fehmi Cirak, Jaime E. Cisternas, Alberto M. Cuitiño, Gerhard Ertl, Philip Holmes, Ioannis G. Kevrekidis, Michael Ortiz, Harm Hinrich Rotermund, Michael Schunack, Janpeter Wolff.

Materials and methods:

The catalysts are ultra-thin platinum single crystals Pt(110), supplied by Jacques Chevallier, Department of Physics and Astronomy, University of Aarhus. They are created by evaporating the platinum metal onto dissolvable sodium chloride single crystal supports with a suitable lattice size. By heating the NaCl crystals to about 650 K, allowing fast surface diffusion, the formation of metal islands is prevented. After reaching their desired thickness, the Pt(110) single crystals are removed from their salt support by dissolving the sodium chloride in a Petri dish filled with ultra pure water. As a result the platinum films float on the water held in place by surface tension. Then 12 × 12 mm Pt support plates, 1 mm thick and each with a conical hole, 4mm diameter at the top, are used to lift the ultrathin platinum single crystals off the water surface. During the drying process the films are cold-welded onto the support plates by adhesive forces. Across the holes of the support plates the single crystals are self-supporting (Fig. 1A).

The single crystal thicknesses were originally about 300 nm; after preparation under ultra high vacuum (UHV) conditions by gentle Ar-ion sputtering and annealing cycles, they wereon average 200 nm thick. The quality of the cold-welding, as determined by the wrinkles along the circumference of the hole varied substantially from sample to sample. Surface preparation quality was checked with low-energy electron diffraction (LEED). The temperature of the support was sustained by radiation from a halogen bulb (max. 250 W) below the sample, while the reactants, O_2 and CO, were introduced at low pressures into the chamber above the crystal. The reaction chamber was a constantly-pumped open flow system. Within a range of parameter settings for the partial pressures of the reactants, the ultra thin crystal deforms and begins oscillating between buckled and flattened states.

Because of the much higher thermal inertia of the 1□mm plate, only the central self-supporting part of the ultrathin single crystal can heat up rapidly during increased reaction. The support temperature remains constant throughout the experiment, thus restricting the thermal expansion of the ultrathin crystal. This then leads to the buckling observed in our experiments and in the modeling.

Supporting text

Modeling of the Chemo-Thermo-Elastic Dynamics:

In modeling the chemo-thermo-elastic dynamics, we start by considering the coupling of chemistry and heat transport, effectively ignoring buckling of the catalyst. The reaction-diffusion equations describing the spatiotemporal dynamics of the adsorbates (CO and O) on the Pt surface are based on the standard mechanistic model (S1):

$$\begin{aligned}
\frac{\partial u}{\partial t} &= k_u s_u p_{CO}[1 - (\frac{u}{u_{\text{sat}}})^3] - k_{\text{des}} u - k_r uv + \nabla \cdot (D_u \nabla u) \\
\frac{\partial v}{\partial t} &= k_v p_{O_2}[w s_{v1} + s_{v2}(1 - w)](1 - \frac{u}{u_{\text{sat}}} - \frac{v}{v_{\text{sat}}})^2 - k_r uv \qquad (1) \\
\frac{\partial w}{\partial t} &= k_{ph}(f(u) - w),
\end{aligned}$$

u, v are the surface concentrations of adsorbed CO and O, respectively. The surface reconstruction variable *w*, describing the CO-coverage dependent lifting of the 2□1 surface phase, is coupled to the CO surface concentration *u* through

$$f(u) = \begin{cases} 0 & u \le 0.2 \\ \frac{1}{0.0135}(u^3 - 1.05u^2 + 0.3u - 0.026) & 0.2 < u < 0.5 \\ 1 & u \ge 0.5. \end{cases} \qquad (2)$$

The experimentally observed temperature variations of 10–30 K can cause dramatic qualitative changes (multiplicity, oscillations, pattern formation) in the isothermal model, due to the exponential (Arrhenius) temperature dependence of the kinetics, via the desorption, reaction and phase change rates (S2):

$$k_{des}[T] = k_{des}^{0} \exp(-E_{des} / R_{gas} T)$$
$$k_{r}[T] = k_{r}^{0} \exp(-E_{r} / R_{gas} T)$$
$$k_{ph}[T] = k_{ph}^{0} \exp(-E_{ph} / R_{gas} T).$$

Details of the continuum mechanical modeling of elastic deformations can be found in (S3).

Finite Element Computation of the Thermo-Elastic Shell Response:

In modeling the elastic shell response, we follow a conventional semi-inverse approach based on a hypothesis regarding the reduced kinematics of the shell body followed by constrained minimization of the three-dimensional potential energy. The basic kinematic assumption is that the deformed shell body is described by the ansatz:

$$\mathcal{B} := \left\{ \boldsymbol{\varphi} \in \mathbb{R}^{3} \;\middle|\; \boldsymbol{\varphi} = \mathrm{x} + \zeta \boldsymbol{n}, \quad \zeta \in [-h/2,\ h/2] \right\},$$

where $\boldsymbol{\varphi}$ is the position vector of a material point within the shell body in its deformed configuration, $\boldsymbol{n}$ is the unit normal vector to the deformed middle surface x, and h is the shell thickness. The Kirchhoff-Love strain energy density of the elastic shell is defined to be:

$$\mathcal{W}(\mathbf{C}, \mathbf{B}) = \mathcal{C}\left[h\, \mathcal{W}_{m}(\mathbf{C}, \mathbf{B}) + \frac{h^{3}}{12} \mathcal{W}_{b}(\mathbf{C}, \mathbf{B}) \right].$$

The strain tensors ε and κ depend on the first and second fundamental forms of the shell middle surface, respectively. Hence, the bilinear form a_m is associated to the membrane response and a_b to the bending response. The material is characterized by the constant C and is defined in terms of the Young's modulus and Poisson's ratio.

Thermal loading of the shell is introduced by a modification of the membrane strain tensor:

$$\varepsilon^{emp} = \alpha \Delta T \, \mathbf{I},$$

where α is the heat expansion coefficient and ΔT the temperature differential. Hereby, we make a constant temperature distribution assumption along the shell normal.

The stable equilibrium configurations of the shell now follow from the principle of minimum potential energy:

$$\inf_{x \in V} \int_{\Omega} W\left(\varepsilon^{emp}(x), \kappa(x)\right) d\Omega \, . \tag{3}$$

The conforming finite element discretization of the energy functional, incorporating the first and second fundamental form of the surface, requires shape functions belonging to the Sobolev space H^2. Subdivision surfaces deliver, in a particularly natural and efficient way, H^2 (smooth) shape functions on general unstructured meshes (S4, S5). In particular, the interpolating shell middle surface is entirely determined by the nodal coordinates of the shell:

$$x_h = \sum_I N^I x_I \, ,$$

where N^I are the shape functions and x_I are the nodal coordinates of the finite element discretized shell middle surface. Introducing the discretization into (3) yields a discrete system of equations. In our numerical computations, we apply the dynamic relaxation

technique for computing the equilibrium configurations. The energy of the continuous as well as the discretized system may be expected to have numerous metastable local minima with energies exceeding the minimum attainable energy. Although certain features of the presented solution, such as the shape and number of folds, are correctly represented, the convergence of the finite element solution to the minimum attainable energy cannot be guaranteed due to the strong non-convexity of the energy functional. The same restrictions also apply to any other approximation scheme for the present problem.

Scaling Relations for the Number and Height of the Ridges:

In this section we briefly describe the theory leading to the scaling relations for the folding wavelength and its corresponding amplitude, which are plotted in Fig. 2 L and M respective-ly. These relations are obtained by minimizing the total deformation energy of the film due to stretching and bending ($\Pi = \Pi_m + \Pi_b$) using the theoretical framework given in (S6, S7), which is based on von Kármán plate theory. In the search for obtaining the optimal folding wavelength we adopt a construction characterized by two regions (Fig. S2a).

The first region is the central zone (Fig. S2b) with ridges perpendicular to the maximum compressive (positive) strain:

$$\varepsilon_1^*(\Delta T) = -\varepsilon_1^0 + \alpha \Delta T, \qquad \text{or parallel to the minimum one}$$

$$\varepsilon_2^*(\Delta T) = -\varepsilon_2^0 + \alpha \Delta T, \tag{4}$$

where $0 > -\varepsilon_1^0 > -\varepsilon_2^0$ are the initial tensile (negative) pre-strains along x_1 and x_2 respectively, α is the thermal expansion coefficient, and ΔT is the temperature differential. The second region is the annular zone (Fig. S2d) necessary to enforce the compatibility of

the out-of-plane displacements $w(x_1, x_2)$ [NOTE: w has been used in section "Modeling of the Chemo-Thermo-Elastic Dynamics" to denote the state of the surface reconstruction] of the inner region with the zero-displacement condition at the boundary of the film.

The inner region, covering an area Ω_i, is composed by flat panels with characteristic slopes:

$$k = \pm [2 (\gamma_1^* + \gamma_2^*)/\beta]^{1/2}, \tag{5}$$

along the x_1 direction (Fig. S2c). This construction minimizes the stretching energy *density* given by the constrained von Kármán theory

$$\Phi_m [w(x_1, x_2)] \quad \{1/4 [|\nabla w|^2 - 2 (\gamma_1^* + \gamma_2^*)]^2 + (1 - \nu) w_{,2}^2 (\gamma_1^* - \gamma_2^*)\} + \Phi_{min}, \tag{6}$$

where h is the thickness of the film, $\nabla w = (w_{,1}, w_{,2})$ is the gradient of w, ν is the Poisson ratio and Φ_{min} is a term independent of w. The total energy in the inner region then becomes proportional to $\Phi_{min} \Omega_i + \Phi_b$, where Φ_b is expressed in the thin film limit as $\Phi_b \quad T D N$, and $T \quad h k^3$ (S8) is the bending energy per unit *length* of a sharp fold, D is the diameter of the circular film and N is the number of folds. The outer region, covering an annular area Ω_0 with a width of the order of D/N (Fig. S2d), is also composed by flat panels with a characteristic slope k but in this case along the x_2 direction. These closure domains contain a membrane energy of:

$$\Phi_m^{\text{ClosureDomain}} \quad [(1 - \nu) k^2 (\gamma_1^* - \gamma_2^*) + \Phi_{min}] \Omega_0,$$

which is obtained by replacing $w_{,1} = 0$ and $w_{,2} = k$ into Eq. (6) and multiplying by the area of the closure domains.

Under these assumptions the number of folds that minimizes the total energy over the inner and outer regions can be expressed as:

$$N \quad [D/h\,(1-\nu)\,(\varepsilon_1^* - \varepsilon_2^*)/k]^{1/2}.$$

Replacing the expressions for the strains Eq.(4) and for the characteristic slopes Eq. (5) into the previous relation, we obtain

$$N \quad K\,(1-\nu)^{1/2}\,[\alpha\,\Delta T / \varepsilon_2^0\,(\rho+\alpha)/(1+\rho)]^{-1/4}, \qquad \text{(L)}$$

where $\rho = \varepsilon_1^0 / \varepsilon_2^0 < 1$ is the initial anisotropy ratio and

$$K = [D/h\,(1-\nu)]^{1/2}\,\{\varepsilon_2^0 / [2\,(1+\nu)]\}^{1/4}$$

groups all the non-essential terms for studying the evolution of N with with ΔT and ρ.

It is worthwhile to mention that in Eq. (L), the term

$$\Delta T_c = (\varepsilon_2^0 / \alpha)\,[(\rho+\alpha)/(1+\rho)]$$

plays the role of a *critical* temperature differential marking the initiation of the wrinkling process.

Finally, the characteristic amplitude for a given folding wavelength can be simply estimated by

$$A \quad k\,D/N. \qquad \text{(M)}$$

The relations (L) and (M), with $\nu = 0.38$, $\alpha = 2.98 \times 10^{-5}$ and $\varepsilon_2^0 = 4 \times 10^{-4}$, have been used to generate the panels (L) and (M) in Fig. 2 respectively.

Supporting figures

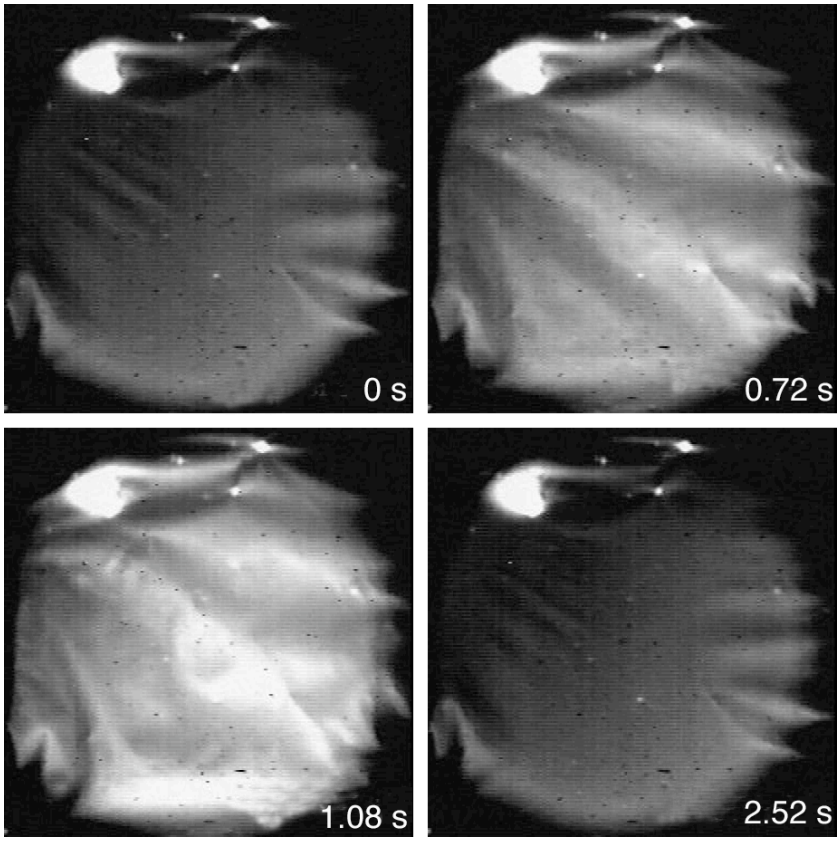

Fig. S1. IR images, using an f = 100 mm Germanium objective and a cooled InSb array sensitive for 3 - 5 μm radiation. p_{O_2} = 5 x 10^{-3} mbar, p_{CO} = 1.5 x 10^{-3} mbar. T_{supp} = 528 K, T increases about 30 K, Size 4.4 □ 4.4 mm. These IR images are taken at half the oxygen partial pressure compared to the one of Movie S1 and of Fig. 1B of the printed paper.

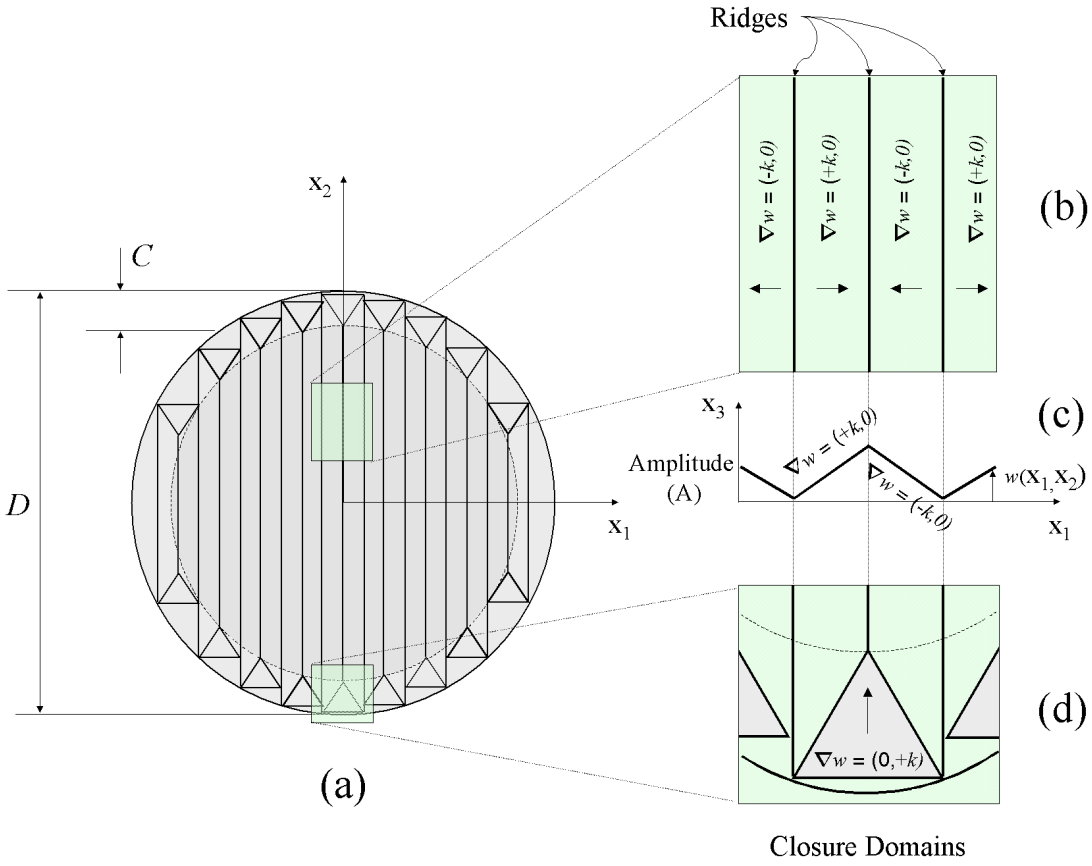

Fig. S2. Schematic of the construction adopted to determine the scaling governing the number of folds (N) and amplitude (A) with the temperature differential for different degrees of initial tensile pre-strain anisotropy.

References:

S1. K. Krischer, M. Eiswirth, G. Ertl, *J. Chem. Phys.* **96**, 9161-9172 (1992).

S2. J. Cisternas, P. Holmes, I. G. Kevrekidis, X. Li, *J Chem. Phys.* **118**, 3312-3328 (2003).

S3. J. Cisternas, P. Holmes, I.G. Kevrekidis, *Physica D* **177**, 71-100 (2003).

S4. F. Cirak, M. Ortiz, P. Schroeder, *Int. J. Numer. Methods in Eng.* **47**, 2039-2072 (2000).

S5. F. Cirak, M. Ortiz, *Int. J. Numer. Methods in Eng.* **51**, 813-833 (2001).

S6. G. Gioia, M. Ortiz, *Adv. Appl. Mech.* **33**, 119-192 (1997)

S7. G. Gioia, A. DeSimone, M. Ortiz, A. M. Cuitiño, *Proc. R. Soc. Lond. A*, **458**, 1223-1222 (2002)

S8. L. Modica, *Arch. Rational Mech. Anal.* **98,** 123-142 (1987)